TURBULENCE MEASUREMENTS FOR WIND-TURBINE SITING ON A COMPLEX TERRAIN

Constantine J. Strataridakis[*]
S.A.M.-High Technology Consulting and Applications S.A.
1770 str. No. 12, Heraklion GR-71202, GREECE

Bruce R. White[†] and Andreas Greis[‡]
Department of Mechanical and Aeronautical Engineering
University of California
Davis CA. 95616, USA

Abstract

Mean velocity and turbulence measurements were used for the wind-turbine siting: A scaled model of the site was tested in the UC Davis Atmospheric Boundary Layer wind tunnel. The surface of the model was scanned at various heights, using hot-wire anemometry. Contour plots of the turbulence intensity and the wind power were generated, respectively. The pattern of the wind-tunnel data was verified by field measurements using a hot-film probe positioned on a 4 m mobile mast. The results were compared with the output of a widely used wind-resource analysis PC-program. It is concluded that turbulence measurements over a site, could indicate quickly and reliably, the suitable positions of the wind-turbines in a wind-farm, taking into consideration that turbulence does not require long-term measurement periods, as it is the case with wind speed. Also, wind-tunnel modelling is a valuable tool in the process of wind energy resource assessment and wind-turbine siting.

Introduction

Wind-turbine siting[1,2,3] on a complex terrain is an expensive and time consuming evaluation process, especially when the area under investigation is large, i.e., several km^2. Studies conducted by the European Union (EU) concluded that there are suitable sites within the EU for 400 GW utilizing wind turbines. These turbines could produce 4000 TWh of electricity per year, which is approximately three times Europe's present electricity consumption.

Although global resource estimates give a good survey of the general wind-energy distribution, more detailed information is required to quantify the wind resource in specific areas. The performance of a wind turbine is completely governed by its site, since the wind varies with location, especially on a complex terrain, the meteorology and the season of the year.

Due to the complexity of the wind field over a complex terrain, wind-turbine performance cannot be predicted accurately without wind measurements on site. Multiple wind measurement stations are needed for a long period of time (several years), in order to accurately assess the wind-energy content over the particular site. Since the wind speed varies with height, measurements have to be performed at hub heights of the wind turbines. Also, wind-profile measurements should be made, in order to determine the wind shear at critical locations of the site.

Most wind-farm developers are using a single weather station, strategically located on the site, for determining site wind conditions. For the detailed calculation of the wind-speed and wind-energy content over the site, various widely-used computer codes are utilized[4,5].

Therefore, it is necessary to incorporate techniques to minimize the amount and duration of on-site measurements for the first wind-potential estimates over a large and complex site. Among these techniques are numerical and physical modeling; both, being very helpful for site

---

[*] Managing Director, Senior Member AIAA
[†] Professor, Fellow Member AIAA.
[‡] Graduate student; on exchange program from University of Aachen Germany.

evaluation, however, multiple direct measurements on the site are necessary to confirm the results of the modeling.

Numerical models use equations that describe the complex interaction between the atmosphere and the earth surface to calculate with given data the wind velocities in other locations where there are no wind observations made. The accuracy of these solutions depends on the amount and quality of the data and the simplified equations which are used for the model.

Physical modeling on the other hand uses the possibility of simulating full-scale winds by means of a wind tunnel. A model of the terrain is placed in a suitable wind tunnel and velocity measurements are conducted. It is important to note that wind tunnels are only able to simulate the air flow in the lowest few hundred meters of the atmosphere. However, wind-tunnel modeling is superior to currently available and broadly used simple numerical models, since these cannot use the strength of the Navier-Stokes equations under random initial conditions. Corrsin (1961) estimated that it would require a memory size of $\sim 10^{13}$ bytes to handle the full complexity of the equations, which is still beyond the capability of present day computers.

In this work both techniques were applied to conduct preliminary valuations of the wind energy potential on a predetermined site: On the southern coast of Crete, the largest Greek island, a 20 MW Wind-Farm project is under development. For this project, a 5 km^2 mountainous land is available. The single weather station on the site has shown that the yearly average wind is approximately 9.0 m/s at 10 m above ground level. The prevailing winds are mostly North and to a lesser extend South. North of the site, extends a large valley (10 km across), while after 4 km to the south, one meets the high cliffs (500 m elevation) of the southern coast of the island.

Presently, a 1:5,000 scaled model (Figure-1 and Figure-2) of a portion of the site was tested in the University of California, Davis Atmospheric Boundary Layer Wind Tunnel (ABLWT) (Figure-3) for the two primary wind directions, north and south. Hot-wire anemometry was used to perform velocity and turbulence measurements at 127 locations over the model. At every location, measurements were made at five different heights, corresponding to 20, 30, 40, 50 and 60 full-scale meters, respectively.

The results of the wind-tunnel tests were qualitatively compared with the output of a standard wind-analyzing program (WASP-Wind Atlas Analysis and Application program[5]), which uses meteorological data, the site topography and roughness as input. In the end, the regions of high wind energy within the site were identified.

For completeness, the wind-tunnel data were verified by field measurements using a hot-film probe (DANTEC) positioned on a 4 m mobile mast. Velocity and turbulence measurements were acquired at several locations on the site.

Wind structure and statistics

Nature of atmospheric winds

The structure of the wind varies between different sites depending on the climate of the region, the surface-roughness conditions and the topography. Since the 1970's significant progress has been made in understanding of the structure of the wind: The winds, in macro-meteorological sense, are movements of air masses in the atmosphere. Partly, these movements are generated by temperature variations within the atmosphere, which are due to differential solar heating. These temperature variations, along with pressure gradients and centrifugal and Coriolis forces, influence the movement of the air masses.

The atmospheric boundary layer

The lowest region of the atmosphere is known as the planetary or atmospheric boundary layer (ABL) and extends from 300 m to 2000 m from the surface. This region is of importance for most engineering problems. The most frequent exceptions from the boundary-layer flow are separation in the lee of hills, storms and tornadoes.

The air flow in the ABL is retarded by surface roughness and large obstructions, thus, the mean wind speed increases with height. Additionally, the atmospheric motion in the boundary layer is influenced by Reynolds stresses, produced by the vertical exchange of momentum due to turbulence. Turbulence, which is of mechanical or thermal origin, also causes rapid changes in the wind velocity over a wide range of frequencies and amplitudes, commonly called gusts. Turbulent fluctuations are random in character and may be analyzed by statistical methods. Also, at different heights, these fluctuations are correlated, the correlation being stronger for small separations and at low frequencies.

Above the ABL the wind is independent of the surface influences and the wind speed is only determined by the pressure field, as well as the latitude position.

Mathematical equations and definitions which describe quantitatively the motion of wind, form the following sections. In these mathematical descriptions it has been assumed, that the wind is over flat, level terrain with uniform surface cover.

The mean wind speed

The mean wind speed is the averaged wind speed over time. The average has to be taken to separate the short-

American Institute of Aeronautics and Astronautics

term fluctuations due to turbulence from the long-term changes.

The mean wind speed is defined as

$$\overline{U} = \frac{1}{T} \int_{to-T/2}^{to+T/2} U(t)dt \qquad (1)$$

where U(t) is the instantaneous wind speed component along the average wind direction at time t_0, and T is the time interval over which the average is taken.

T is determined by spectral analysis of the wind-speed time series. The long-term spectra of kinetic energy of the horizontal wind give the reason for choosing an averaging period of one hour. This is the time period on which most of the meteorological data is based.

Except for small differences, other spectra show the same characteristics. On the low-frequency side of the spectrum, the structure is determined by the large-scale synoptic movements of air masses. The cycle is about four days long. On the other side of the spectrum, lies the high-frequency side. This side is influenced by the atmospheric turbulence and forms the micro-scale range. The peak energy is centered around 1 minute. Between these two peaks' lies a gap, which extends from a period of 10 minute to 2 hours. The energy level is very low in this region. By choosing an averaging period lying in the gap, the synoptic variation can be separated from those caused by turbulence. Hence, it is suggestive to take an averaging period of around one hour.

Prandtl logarithmic law

The planetary boundary layer consists of several layers with different set of flow parameters. However, the layers of interest for most engineering problems are the *surface* and *Ekman* layers.

The height of the surface layer is approximately 50 to 100 m. In this region the vertical variation of shear stress can be neglected without significant loss of accuracy with regards to the mean velocity profile. A good representation of the variation of the mean wind speed with height gives the Prandtl logarithmic law[6]

$$\overline{U}(z) = (u_* / k)\ln(z/z_0) \qquad (2)$$

where $\overline{U}(z)$ is the mean wind speed at height z, u_* is the friction velocity, k is the von Karman constant, which is equal to 0.4 and z_0 is the roughness length determined by the surface condition of the surface. The friction velocity u_* changes with surface roughness and overall wind speed.

Comparison between measurements and calculations of the log-law model showed that the model can describe the change of mean wind speed in the surface layer with reasonable accuracy.

The best way to apply Equation (2) is to eliminate the friction speed. This can be done by using the mean-wind speed measured at a reference height, commonly 10 m. Thus, one obtains

$$\frac{\overline{U}(z)}{\overline{U}(H)} = \frac{\ln(z/z_0)}{\ln(H/z_0)} \qquad (3)$$

The only remaining unknown value in this equation is the roughness height z_0. The appropriate value for z_0 is usually found by comparison of the surface structure of the site to regions where the roughness length has been determined. In some areas, z_0 is changing by an order of magnitude between summer and winter due to different vegetation. This has to be kept in mind when investigating a prospective wind-turbine site. Equation (3) can be useful for estimating z_0; however it should be treated with caution.

Power-law model

The Ekman layer continues the surface layer to the top of the boundary layer. In this region, the Coriolis force increases and the shear stress decreases with height. At a height of approximately 500 to 2,000 m the influence of the shear stress vanishes. Another phenomenon is the variation of the wind direction in the different heights of the layer, known as Ekman spiral. The direction of the wind rotates from nearly parallel to the isobars at the top of the layer to 15-30° towards the lower pressure region near the surface.

In some situations when simple estimates of the distribution of the mean wind speed with height are required, it is appropriate to use the empirical-power-law model:

$$\frac{\overline{U}(z)}{\overline{U}(H)} = \left(\frac{z}{H}\right)^\alpha \qquad (4)$$

in which $\overline{U}(H)$ is the mean wind speed at reference height, H, and the exponent, α, depends on the range of height being covered and the surface roughness. The height for the reference speed is usually 10 m.

A relationship between surface roughness and exponent α is given by[1]

$$z_0 = 15.25\exp(-1/\alpha). \qquad (5)$$

This prediction is accurate within a few percentages over the range of roughness lengths of interest. It is important to note that the power law has no theoretical foundations, however, it is often used by engineers. Using one or the other form, to find the mean wind speed distribution, one has to solve the task of estimating z_0 or α.

The difficulty in analyzing wind-speed data lie in the fact that the roughness length may be different for different wind directions and it can change over the year due to variation

4

of vegetation cover. Thus, the hourly taken mean wind speeds are themselves strongly dependent on the wind direction and the season of year. When averaging the mean-wind speed over a long period i.e., a year, these dependencies vanish and they do not influence the estimation of the wind potential of a site. Also, difficulties arise when extrapolating the annual wind speed from one height to another, therefore it is suggested to take wind-speed measurements at hub heights.

Considering all these difficulties in the actual measurement of the wind resource, most often the power-law model is used for the wind-speed profile calculations.

Wind-speed-distribution function

The wind-speed probability-density function or the frequency distribution of wind speed, F(U), is used in wind energy investigations. The Weibull distribution is the most widely used

$$F(U) = (k/c)(U/c)^{k-1} \exp[-(U/c)^k] \tag{6}$$

where F(U) is the frequency of occurrence of wind speed U, c is the scale parameter and k is the shape parameter. The parameter c has the dimensions of speed, m/s.

Another important distribution is the duration curve. It gives the probability of the wind speed exceeding a certain value. The cumulative Weibull distribution gives

$$f(U) = \exp\left[-\left(\frac{U}{c}\right)^k\right] \tag{7}$$

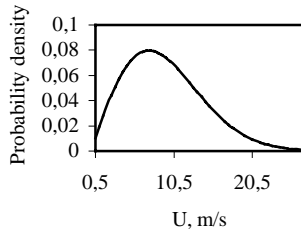In the present study, the Weibull distributions used are presented in Figures 4 and 5, respectively.

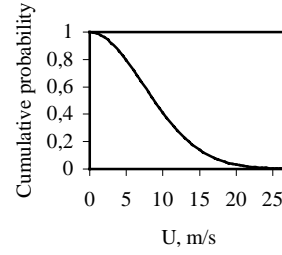*Figure-4. Probability density function with Weibull coefficients c=10.5 m/s and k=1.95.*

Figure-5. Cumulative probability curve with Weibull coefficients c=10.5 m/s and k=1.95.

Turbulence

Turbulence is quasi-deterministic and the statistical methods are used for its analysis. Turbulence is described by all fluctuations with frequencies higher than the mean wind speed variations; thus, it is defined as the deviation of the instantaneous wind speed U(t) from the quasi-steady mean wind speed $\overline{U}$.

The variance σ_u^2 stands for the variability of the wind speed and is defined as

$$\sigma_u^2 = \overline{u^2} = \frac{1}{T} \int_{t_0-T/2}^{t_0+T/2} [U(t) - \overline{U}]^2 dt \tag{8}$$

Using this definition, the turbulence intensity I_u is

$$I_u = \frac{\sigma_u}{\overline{U}} \tag{9}$$

Holding the height fixed, the variance increases with increasing wind velocity. Nevertheless, turbulence intensity decreases usually with height, since the mean wind speed increases more rapidly than the variance. More detailed information about the structure of the turbulence is given by Hinze[7].

Wind Power

Wind is air in motion. The kinetic energy of the wind is

$$E_{kin} = \frac{1}{2} \cdot m \cdot U^2 \tag{10}$$

where m is the air mass and U the wind speed.

The power of the wind is the kinetic energy passing through an area A in unit time, or

$$P = \frac{1}{2} \cdot \rho A U \cdot U^2 = \frac{1}{2} \cdot \rho A U^3 \propto U^3 \tag{11}$$

This is the total available power of the wind for conversion to mechanical and consecutively to electrical by the blades and the generator of a wind turbine, respectively. The power of the wind is very sensitive to the wind speed, since it is dependent on the wind speed to the third power.

Wind-turbine siting

Wind-turbine siting on a large (5 km^2) complex terrain land is a very lengthy and costly procedure. The acquisition of reliable meteorological data is essential to wind-farm development. By placing anemometers strategically on prominent location over the site, the general suitability of the site could be determined. However, assessing the extent of the usable wind resource, the evaluation process is considerably more involved[8].

The first step for the determination of the land-suitability for wind-farm development is the acquisition of *meteorological data* within the site, preferably at wind-turbine hub heights. Second, incorporating the meteorological data, *numerical models* could be used for estimating the flow field over the terrain. The models use the equations of motion to describe the air flow over the earth's surface. The accuracy achieved in this model depends on the density of the meteorological data measured and the amount of inherent realism in the equations used in the model. Third, *wind tunnel testing* could be utilized for physically simulating the flow field over the potential site. A model of the site of interest is placed in a wind tunnel and wind-speed measurements can be taken. However, the modeled site can only be a few tens of kilometers in size and the portion of the atmosphere to be studied must be the lowest few hundred meters, in order to guarantee reasonable results. Considering these constraints, wind-tunnel simulation can be a useful tool in the wind-turbine siting process.

For terrain with very complex topography, where the height changes of the order of the size of the wind turbines, it is necessary to conduct additional field measurements, especially turbulence measurements, at critical locations on the site, for further evaluation of the physical and numerical simulation results. On - site turbulence measurements at hub heights are also very important for the investigation of gust events at different locations. Wind-turbine siting over gusty area could adversely effect the wind turbine operation and the turbine service life. Therefore, locations with high turbulence intensity should be avoided.

Lastly, knowing the flow-field over the site, the economic value of the wind-generated electricity should be assessed for the specific wind turbines.

In the present study, emphasis is given in turbulence measurements and since wind-tunnel testing is a powerful tool in wind-turbine siting, physical modeling is described in more detail, next.

Wind-tunnel simulation

Physical modeling[9,10,11,12,13] in a wind tunnel has great flexibility for simulation of atmospheric boundary layers. Uniform-surface boundary layers and local flow around obstacles can be realized for high complicated surface conditions like urban areas.

The ability of physical modeling to simulate flow over small-scale terrain features in nearly neutral flow is still superior to available numerical models. Numerical modeling is restricted and usually used for non-complicated boundary conditions and uniform surface conditions. Therefore, physical modeling can be helpful in the process of turbine siting.

Since the models used in a wind-tunnel simulation study are orders of magnitude smaller than the full-scale object, it is not obvious that the results obtained will be corresponding to nature. Results from wind-tunnel tests are representative to full-scale conditions, as long as certain parameters for the model and the full-scale object, respectively, are equal.

For exact modeling, all the non-dimensional similitude parameters should be matched, which is impracticable, if not impossible. Hence, the key similitude parameters have to be selected, which are dominant for the investigated case. However, one needs to first find all parameters, before one can neglect some of less important ones. By nondimensionalizing the equation of motion one can obtain the similarity parameters.

Requirements for the simulation of the atmospheric boundary layer

The equations of motion build the starting point for the similarity analysis. The fluid motion can be described by the following time-averaged equations:

Conservation of mass

$$\frac{\partial \overline{U}_i}{\partial k_i} = 0 \quad \text{and} \quad \frac{\partial \rho}{\partial t} + \frac{\partial (\rho \overline{U}_i)}{\partial x_i} = 0 \qquad (12)$$

Conservation of momentum[9]

$$\frac{\partial \overline{U}_i}{\partial t} + \overline{u}_j \frac{\partial \overline{U}_i}{\partial x_j} + 2\varepsilon_{ijk}\Omega_j \overline{U}_k = -\frac{1}{\rho_0}\frac{\partial \overline{\delta P}}{\partial x_i} - \frac{\overline{\delta T}}{T_0}g\delta_{i3} + \nu_0 \frac{\partial^2 \overline{U}_i}{\partial x_j^2} + \frac{\partial(\overline{-u_j u_i})}{\partial x_j} \quad (13)$$

The mean quantities are represented by capital letters and the fluctuating values by small letters. δP is the deviation from the pressure of a neutral atmosphere, ρ_0 and T_0 are density and temperature of a neutral atmosphere and ν_0 is kinematic viscosity. The equation is time averaged. Since the Boussinesq density approximation is made, the application of the equation is restricted to flow where $\overline{\delta T} << T_0$.

Conservation of energy

$$\frac{\partial \overline{\delta T}}{\partial t} + \overline{u}_i \frac{\partial \overline{\delta T}}{\partial x_i} = \left[\frac{\kappa_0}{\rho_0 c_{p_0}}\right]\frac{\partial^2 \overline{\delta T}}{\partial x_k \partial x_k} + \frac{\partial(-\overline{\theta u_i})}{\partial x_i} + \frac{\overline{\phi}}{\rho_0 c_{p_0}} \qquad (14)$$

Here ϕ is the dissipation function, $\overline{\delta T}$ is the deviation of temperature from the temperature of a neutral atmosphere, κ_0 is the thermal diffusivity and c_{p0} is the heat capacity.

Nondimensinalizing these equations we obtain:

Continuity

$$\frac{\partial u_i'}{\partial k_i'} = 0 \;\; \text{and} \;\; \frac{\partial \rho'}{\partial t'} + \frac{\partial(\rho' u_i')}{\partial x_i'} = 0 \qquad (15)$$

Momentum

$$\frac{\partial \overline{U}_i'}{\partial t'} + \overline{U}_j' \frac{\partial \overline{U}_i'}{\partial x_j'} + \frac{2}{Ro}\varepsilon_{ijk}\overline{U}_k'\Omega_j' = -\frac{\partial \overline{\delta P}'}{\partial x_i'} + \frac{1}{H^2}\overline{\delta T}'\delta_{3i} + \frac{1}{Re}\frac{\partial^2 \overline{U}_i'}{\partial x_j'\partial x_j'} + \frac{\partial(-\overline{u_j'u_i'})}{\partial x_j'} \qquad (16)$$

Turbulent energy equation

$$\frac{\partial \overline{\delta T}'}{\partial t'} + \overline{U}_i'\frac{\partial \overline{\delta T}'}{\partial x_i'} = Pr\cdot\frac{1}{Re}\frac{\partial^2 \overline{\delta T}'}{\partial x_k'\partial x_k'} + \frac{\partial(-\overline{\theta' u_i'})}{\partial x_i'} + \frac{1}{Re}\cdot Ec\cdot\overline{\phi}' \qquad (17)$$

The nondimensional quantities appearing in these equations are defined as follows:

$$\overline{U}_i' = \overline{U}_i'/U_0 \;;\; u_i' = u_i/U_0 \;;\; x_i' = x_i/L_0 \;;\; t' = tU_0/L_0 \;;\; \Omega_j' = \Omega_j/\Omega_0 \;;\; \overline{\delta P}' = \overline{\delta P}/\rho_0 U_0^2 \;; (18)$$
$$\overline{\delta T}' = \overline{\delta T}/\delta T_0 \;;\; g' = g/g_0 \;;\; \overline{\phi}' = \overline{\phi}/\phi_0$$

The continuity equation gives no similarity parameters. The coefficients in both other equations are the desired similarity parameters:

1. Rossby number: $\;\; R_0 \equiv U_0/L_0\Omega_0 \qquad (19)$

2. Densimetric Froude number: $\; Fr \equiv U_0/(gL_0\delta T_0/T_0)^{1/2} \qquad (20)$

3. Reynolds number: $\; Re \equiv U_0 L_0/\nu_0 \qquad (21)$

4. Prandtl number: $\; Pr \equiv \rho_0 c_{p_0}\nu_0/\kappa_0 \qquad (22)$

5. Eckert number: $\; Ec \equiv U_0^2/c_{p_0}\delta T_0 \qquad (23)$

The Rossby number represents the ratio of advective acceleration to Coriolis acceleration due to the rotation of the earth. Evidently, if the Rossby number is large, Coriolis accelerations are small. In a wind tunnel, which is not rotating, the Rossby number is infinite. In nature, however, the rotation of the earth is of influence in the upper layers of the atmosphere and the Rossby number becomes important to match.

Most modelers have assumed the Rossby number to be large and neglected the terms involving it in the equations of motion i.e., ignored the Rossby number as criterion for modeling. Snyder[12] shows that the characteristic length scale has to be smaller than 5 km to simulate diffusion under neutral or stable conditions in relatively flat terrain. Other researchers discovered similar findings. If the wind tunnel produces a boundary layer of one meter height, the surface layer is extended up to 10 cm to 15 cm above the ground. In this region the velocity spectrum would be accurately modeled. The Rossby number can be ignored in this region.

Since testing is limited to the lower 10% to 15% of the boundary layer, the length in longitudinal direction which can be modeled, has to be no more than a few kilometers.

The square of the Froude number represents the ratio of inertial forces to buoyancy forces. High values of Fr infer that the inertial forces are dominant. Therefore, thermal effects become important for values equal or less than unity. Hence, a neutral stable flow (Fr is infinity) would be easily simulated by an isothermal wind tunnel flow.

The third parameter is the Reynolds number. It represents the ratio of inertial to viscous forces. Commonly, the scale reduction results in a Reynolds number several orders of magnitude smaller than in full scale. The viscous forces are thus more dominant in the model than in nature. No atmospheric flow could be modeled, if strict adherence to the Reynolds number criterion was required. However, several arguments have been made to justify the use of a smaller Reynolds number in a model. These arguments are the laminar flow analogy; Reynolds number independence; and dissipation scaling.

With the absence of thermal and Coriolis effects it has been shown that the scaled model flow will be dynamically similar to the full-scale case if the Reynolds number is larger than a minimum independence value. There exists a large amount of test results supporting this principle. The gross structure of turbulence is similar over a wide range of Reynolds numbers. This is used today by nearly all modelers.

The fourth parameter is the Prandtl number. It is automatically matched in the wind tunnel if the same fluid is been used.

The Eckert number criterion is only of importance in compressible flow, which is not of interest in our case.

Boundary conditions

For proper modeling it is necessary that also certain non-dimensional boundary conditions are equal for model and full-scale. The most important conditions are:

1. The mean normalized velocity; turbulence intensity; and turbulent energy profile.

2. The roughness Reynolds number, $z_0 u_* / \nu$.

3. Jensen's length-scale criterion of z_0/H.

4. The ratio of H/δ for H greater than $H/\delta > 0.2$.

An equal normalized mean velocity profile is obtained by choosing the appropriate surface roughness length for the wind tunnel. This produces the correct power-law exponent, α.

The normalized turbulence intensity profiles have to be matched in the lower portion of the wind-tunnel boundary layer to that of the atmospheric boundary layer. The whole profile cannot be matched due to scaling effects. However, a long flow development section of the wind tunnel results in better agreement of wind tunnel and full-scale normalized turbulence profile. The same is valid for matching the inertial subrange region of the non-dimensional energy profiles between wind tunnel and full scale. The installation of flow spires at the entrance of the wind tunnel will improve the energy spectra and makes possibly, a shorter flow development section necessary.

In wind-tunnel simulation of atmospheric-boundary-layer flow, the mean non-dimensional velocity profile is easiest to match to full scale; more difficult to match is the turbulence intensity, and the most difficult to simulate are the energy spectra profiles. Approximately, one needs 10 to 25 boundary-layer-heights length of fetch to match the mean velocity profile, about 50 boundary layer height lengths to match the turbulence intensity profiles and about 100 to 500 boundary layer height length to match the turbulent energy spectra. However, using spires and other flow tripping devices the necessary flow development length in the wind-tunnel can be reduced to less than 20 boundary layer heights for most engineering applications.

The second boundary condition involves the roughness Reynolds number, $Re_r = u_* z_0 / \nu$. The roughness Reynolds number has to be larger than a critical value, in order to simulate a naturally occurring atmospheric boundary layer. The criterion is: $u_* z_0 / \nu \geq 2.5$ (Sutton, 1949), where u_* is the friction speed, z_0 is the surface roughness length and ν is the kinematic viscosity. A Re_r larger than 2.5 ensures that the flow is aerodynamically rough; flow over an aerodynamically rough surface is Reynolds number independent. Therefore, wind tunnels with a high enough roughness Reynolds numbers simulate full-scale aerodynamically rough flows exactly. To produce a rough surface in the wind tunnel roughness elements are placed on the wind tunnel floor. The height of the elements has to be larger than the height of the viscous sub-layer in order to trip the flow.

To simulate the pressure distribution on objects in the atmospheric wind, Jensen (1958) found that the surface roughness to object-height ratio in the wind tunnel must be equal to that of the atmospheric boundary layer, i.e., z_0/H in the wind tunnel must match the full-scale value. Thus, the geometric scaling should be accurately modelled.

The last condition for the boundaries is the characteristic scale height to boundary layer ratio, H/δ. There are two possibilities for the value of the ratio. If $H/\delta \geq 0.2$, then the ratio has to be matched, if $(H/\delta)_{F.S.} < 0.2$, then only the general inequality of $(H/\delta)_{W.T.} < 0.2$ must be met (F.S. stands for full-scale and W.T. stands for wind tunnel). Using the law-of-the-wall logarithmic profile equation, instead of the power-law velocity profile, this principle would constrain the physical model to the 10% to 15% of the wind tunnel boundary layer height.

Along with these conditions, two other constraints have to be met. The mean longitudinal pressure gradient in the wind tunnel should be zero. Even if high- and low-pressure systems create atmospheric boundary layer flows, the magnitude of the pressure gradient in flow direction is negligible compared to the dynamic pressure variation caused by the boundary layer.

The other constraint is that the model should not take up more than 5% to 15% of the cross-sectional area at any down wind location. This assures that local flow acceleration affecting the longitudinal pressure gradient will not distort the simulation flow.

As stated earlier the whole atmospheric boundary layer cannot be modeled without bringing the wind tunnel into rotation. Thus, the geostrophic wind cannot be simulated in the wind tunnel. In this region, the influence of the rotation of the earth becomes important and cannot be neglected anymore. Therefore, wind tunnel studies are only valid for simulation of the surface layer of the atmospheric boundary layer.

The wind-tunnel facility

In the present investigation, the UC Davis Atmospheric Boundary Layer Wind Tunnel (ABLWT) was used (Figure-3). The wind tunnel was built in 1979. The intention was to design a wind tunnel, which is able to simulate naturally turbulent boundary layers, such as wind flow near the surface of the earth. Therefore, the tunnel requires a long flow development section to produce a mature boundary layer flow at the test section.

The wind tunnel is composed of four sections: the entrance, the flow developing section, the test section, and the diffuser section.

The entrance section is of elliptical shape and provides this way the incoming flow with a smooth contraction area, which minimizes the turbulence. A commercially available air filter follows the contraction area. This filter reduces

American Institute of Aeronautics and Astronautics

large-scale pressure fluctuations of the flow and filters larger-size particle out of the incoming flow. After the filter, a honeycomb flow straightener is used to reduce large-scale turbulence.

The second part of the wind tunnel is the flow development section. It is 12.2 m long. It produces the mature turbulent boundary layer. Four spires placed at the entrance of this section and surface roughness elements placed all over the surface of this section generate a boundary layer of a height of one meter at the test section. The ceiling of the developing section has an adjustable false ceiling and diverging walls, to provide zero-pressure-gradient flow.

The dimensions of the test section are 3 m in streamwise length, 1.7 m high and 1.2 m wide. The test section can be observed from both sides through a framed Plexiglas window and a framed Plexiglas door, which allows access to the test section. The ceiling of the test section can be adjusted to obtain zero-pressure-gradient flow over its length. To introduce a probe in the test-section a three-dimensional traversing system is installed at the ceiling of the test section. The sensor can be moved over almost the whole test section volume. The traversing system is of aerodynamically shape minimizing influences on the flow. The centerline wind speeds within the test section can be adjusted from 1 m/s to 10 m/s.

The diffuser section is 2.44 m long. It has a circular cross section for the fan. The eight-blade, fixed-pitch, 1.83 m-diameter fan is powered by a 56 kW DC motor with controller.

<u>The wind-tunnel characteristics</u>

The boundary layer in the wind tunnel has to be turbulent like the atmospheric boundary layer. This is achieved by roughening the surface, so that the roughness Reynolds number, Re_z, is greater than 2.5. The UC Davis ABLWT satisfies this condition, since the roughness Reynolds number ($Re_z = u_* z_0 / \nu$) is about 40; when the wind-tunnel freestream velocity, U_∞, is equal 3.8 m/s, the friction speed, u_*, is 0.24 m/s and the roughness height, z_0, is 0.0025 m. Thus, with the freestream speed of 3.8 m/s the flow satisfies the Re number independence criterion and dynamically simulates the flow.

The velocity profile in the wind tunnel should be describable by the power law. Equation (4) gives a relationship between a mean velocity, u, at a height, z:

$$\frac{u}{u_\infty} = \left(\frac{z}{\delta}\right)^\alpha \qquad (24)$$

where δ is the boundary-layer height, u_∞ is the inviscid speed at height δ and α is the power-law exponent. The wind-tunnel flow can be conditioned, such that the exponent

α will closely match the full-scale value of α. The mean tunnel velocity profiles for the two cases (north wind and south wind) measured in this study, are displayed in Figures 6 and 7, respectively. The value for α is 0.23 for north wind and 0.33 for south wind, respectively.

In the lower 20% of the boundary layer height, which is governed by a rough-wall logarithmic mean velocity profile,

$$\frac{u}{u_*} = \frac{1}{\kappa} \ln\left(\frac{z}{z_0}\right) \qquad (25)$$

where κ is von Karman's constant. The scaled model should, desirably, contained within this layer. Considering a boundary-layer height of the order of a meter at the test section, the surface layer would be 0.2 m deep. This boundary layer corresponds to a full-scale height of the order of 1 km; and since the highest elevation in the site-model investigated in this study is about 750 m full-scale, the model is contained in this region. This region of the boundary layer is relatively unaffected by the Coriolis force, and it is the only region that can be modeled accurately by the wind tunnel.

The turbulent intensity profile, u'/u versus z, should agree reasonably with the full-scale, particularly in the region where testing is performed.

The maximum values of the UC Davis wind tunnel turbulence intensity range from 35% to 40%. This range is similar to that in full-scale. In Figure-8, the turbulence intensity profile of the wind tunnel boundary layer is shown.

The geometric scale of the model should be determined by the size of the wind tunnel, the roughness height and the power-law index α.

In the present investigation all tests were carried out in the UC Davis ABLWT. This wind-tunnel facility did not have the capability of producing stable boundary layer flow. Further, it is noted that it is not possible to simulate unstable B.L. flows in wind tunnels because the artificial secondary flows, caused by the heating, dominate and distort the longitudinal mean-flow properties, thus invalidating the similitude criteria. However, this is not considered as a major constraint, because the winds that produce energy are sufficiently strong, such that for flow over a complex terrain, the primary source of turbulence is due to mechanical shear and not due to diurnal or heating and cooling effects in the atmosphere.

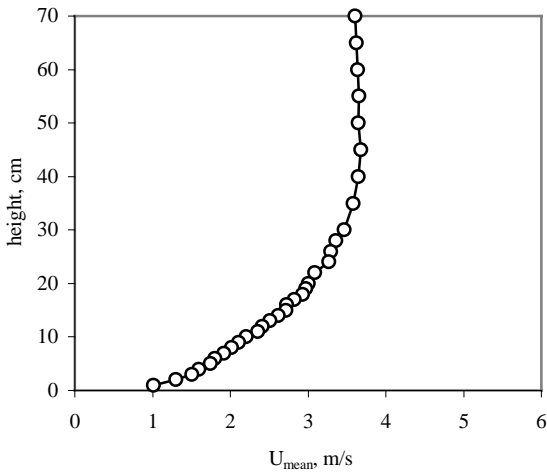American Institute of Aeronautics and Astronautics

Figure-6. Mean velocity profile measured for North wind direction in the wind tunnel. The power law exponent α is 0.23. The reference velocity at 65 cm height is 4.17 m/s.
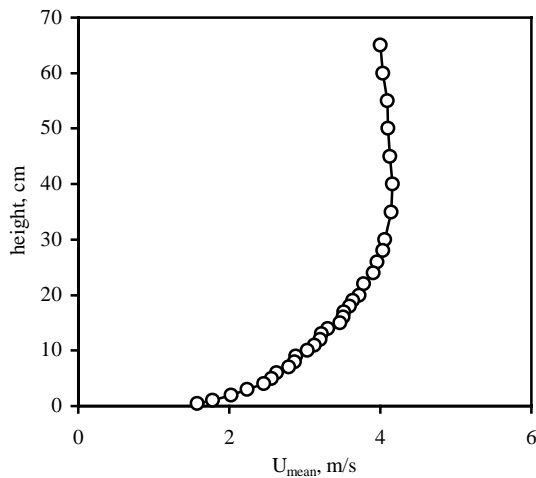

Figure-7. Mean velocity profile measured for South wind direction in the wind tunnel. The power law exponent α is 0.33. The reference velocity at 65 cm height is 3.55 m/s.

Hot-wire anemometry

During the wind-tunnel tests, hot-wire anemometry was used for the mean velocity and turbulence measurements[14]. Figure-9 presents the schematic diagram of the system used: A standard TSI single-sensor (TSI Model 1210-60); a two-channel thermal-anemometry unit with signal conditioner (TSI model IFA 100); and a 12 bit AD converter (IBM Data Acquisition and Control Adapter DACA), driven by an IBM-AT computer. The hot-wire sensor was calibrated with the TSI-1125 calibration unit.
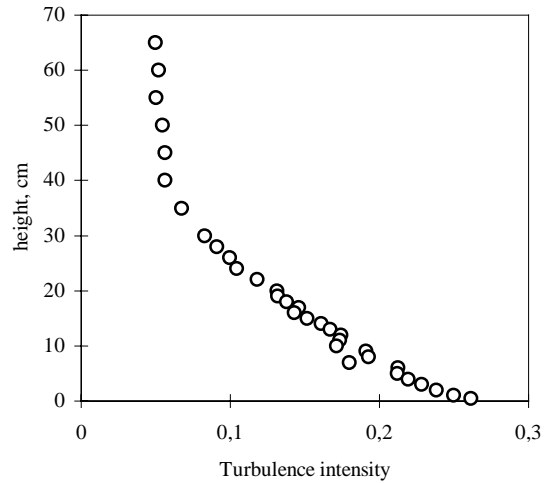
Figure-8. Turbulence intensity profile for north wind direction in the wind tunnel.

The number of velocity samples, over which the mean velocity was averaged, as well as the sampling rate were equal for all wind-tunnel test runs. The number of samples was set to 30,000 and they were taken with a rate of 600 Hz, in order to satisfy the Nyquist sampling theorem, since the tunnel turbulence signal was 300 Hz. Thus the sampling time was 50 sec.
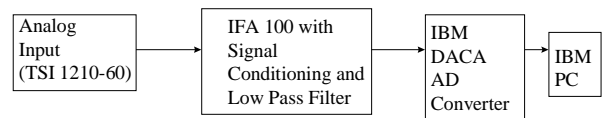
Figure-9. Schematic diagram of the mean velocity and turbulence measurement system.

Field measurements

In the present study, cup-anemometer measurements were performed at 10 m above ground level for several months. A hot-film anemometer sensor (DANTEC) was used to acquire mean wind-speed and turbulence data on several locations within the site. The DANTEC probe was placed on a 4 m mobile mast. Turbulence data were collected at the selected on-site locations for two-days.

American Institute of Aeronautics and Astronautics

Figure-10 presents the wind directional occurrence rate and along with Figures-4 and -5, respectively, give a description of the flow over the site under investigation.

The digitized map for a portion of the site under investigation is presented in Figure-11. The dot indicates the meteorological station site at 10 m above ground level. The crosses show the locations where the movable mast with the hot-film probe was positioned, for the acquisition of the turbulence measurements.

The *WASP* program

The *Wind Atlas Analysis and Application Program - WASP*[5]-; is a PC-computer program for the horizontal and vertical extrapolation of wind data. The program takes into account for its calculations the effects of different roughness conditions, sheltering effects due to nearby obstacles and the influence of the terrain structure.

Using WASP, the wind energy per unit time distribution of the site was calculated, in W/m^2, at the same heights as in the wind-tunnel measurements. The resource file function was applied for each of the five discrete full-scale heights tested in the wind tunnel (20, 30, 40, 50, and 60 m, respectively). The grid area which included the portion of the site was set to 3×2 km^2 (15000 to 18000 m east-west direction and -30000 to -28000 m north-south direction, in cartesian coordinates, that correspond to the map) and a grid size of 50 m was chosen.

Wind-tunnel measurements

The wind-tunnel testing was carried out on a 1:5,000 scaled model of the selected area of the site. The UC Davis ABLWT was used for all experiments. Since the North and South winds are the prevailing ones, as Figure-10 indicates, these two wind directions were simulated in the wind tunnel. The measurements indicated that more than 80% of the wind came from southern or northern direction. This justifies the assumption that all other wind directions have smaller influence in the wind energy distribution on the site.

Over the site model, velocity and turbulence measurements were taken at 127 locations. The locations were ordered in rows running from north to south. The distance between each row was 125 m in full-scale. Figure-12 shows the pattern in which the locations were ordered. To label the locations ordinary point stickers were used.

In every location the velocity was measured at five different heights: 40, 60, 80, 100, and 120 mm, respectively. The corresponding full-scale heights were 20 m, 30 m, 40 m, 50 m and 60 m. To adjust the hot-wire on
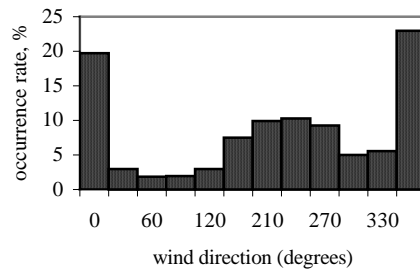
Figure-10. Occurrence rate of wind for different directions.
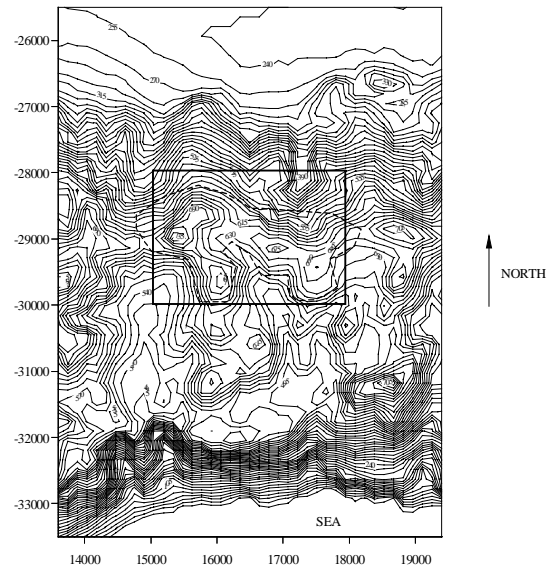

Figure-11. Digitized map of the region of interest. The measurement stations are indicated. The coordinates are in (m). The rectangle indicates the area covered by the wind-tunnel measurements.
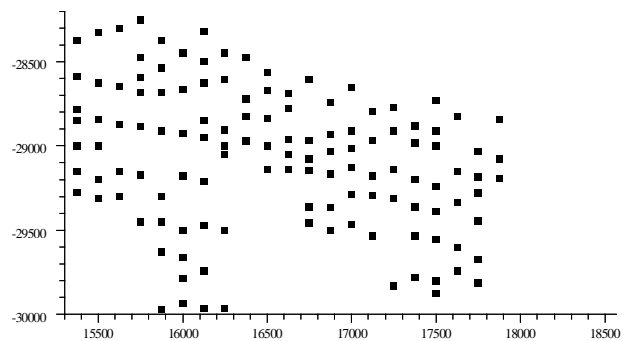

Figure-12. Locations within the site model, where wind-tunnel measurements were acquired. The coordinates correspond to cartesian (m).

the desired height marked tooth sticks were used. These sticks were placed nearby the locations were the velocity

American Institute of Aeronautics and Astronautics

measurements were taken. To avoid flow disturbance caused by the wood sticks the distance between stick and location was set to more than 10 times the diameter of the stick.

To reference the measured wind speeds for different test runs, the freestream wind speed was acquired at a height of 65 cm in the wind tunnel for every test run. The freestream velocity was approximately adjusted to 3.7 m/s. In this study, the mean velocity U_{mean} and the turbulence intensity (TI) data were stored for further analysis.

In addition to the velocity measurements over the site model, the undisturbed velocity and turbulent intensity profiles were measured upstream the model for both wind directions, north and south; Figures-6, 7 and 8 show these results, respectively. For the North direction, i.e., north winds, the power-law exponent α is 0.23; while α equals to 0.33 for the South direction. The undisturbed turbulence intensity profiles are similar for both wind directions.

Uncertainties

Detailed uncertainty analysis is beyond the scope of this study, however, uncertainties in the wind-tunnel measurements were estimated to be:

Quantity	Uncertainty
mean velocity	± 1%
Turbulent Intensity	± 5%
Probe positioning (horizontally)	± 7.5%
Probe positioning (vertically)	± 15%

Table-1. Uncertainty estimates.

The uncertainties in the field measurements were estimated to be twice the above uncertainties with the exception of the vertical probe positioning which was within 5%.

Results

The major scope of this study was to utilize an atmospheric boundary layer wind tunnel as a tool for wind-turbine siting on a large and complex terrain. On-site turbulence field-measurements were performed, in order to qualitatively evaluate the wind-tunnel results. Further and as it is well known, since the turbulence field does not require long-term (several years) observations to be determined[14], it is important to link turbulence measurements to wind-turbine siting.

In the present study, the WASP program was chosen as the numerical tool, since WASP could give indicative results about the wind energy distribution over a site quickly and inexpensively and most importantly, WASP has been a standard tool in wind-siting assessments for wind-farm development in Europe.

For WASP, except for the necessity to input data from preferably several meteorological stations, especially when the site is very large and complex, intuition and long experience is needed for correctly setting up the input parameters of the program; i.e., roughness heights in each wind direction, obstacle definitions etc.

The WASP results are shown in Figures 13 through 17, for the same heights tested in the wind tunnel. The plots present the wind power distribution (energy per unit time) per unit area [W/m^2] over the selected site. Evaluating Figures 13 to 17, it can be observed that there is not a considerable change in the wind energy content with height. Also, the wind-energy field, according to WASP results, follows the complex topography closely. In other words, on the top of the hills the wind energy is high and in the valleys is low.

The mean velocity measurements in the wind-tunnel were used to calculate the relative wind power, $P/P_{ref}=(U/U_{ref})^3$, assuming that the density variation over the site is negligible. The results are presented in Figures 18 through 25 for the full-scale heights 20 m to 50 m, respectively. These plots are valid only inside the boundaries outlined, since within these boundaries all velocity measurements were taken. From these figures it is noticed that the wind energy content increases rapidly with height. The best areas for positioning wind turbines appear to be the areas in ''warm'' colors (yellow and red). To further isolate the best areas, the figures corresponding to the same height should be overlaid; thus, the commonly outlined warm colors indicate the best proposed candidates for wind-turbine sites. This procedure simply gives the integrated result for North and South wind directions, which are the prevailing winds for the site.

Testing the flow over the model for other wind directions would have been necessary, only in the case that these winds were prevailing. In the present investigation, this was not considered necessary, since more that 80% of the time, north or south winds are blowing.

Presently, the pattern of the field measurements appeared to be in a reasonable agreement with the plots of the wind tunnel data. On-site turbulence measurements were taken at 13 locations at 4 m above ground level (Figure-11). The results traced the turbulence intensity patterns for the north wind, since the wind was steadily north during all field tests. Detailed field-measurement data are not presented in this preliminary investigation.

Comparing wind-tunnel results (considering south and north wind) and WASP program results it can be found that the general structure of the wind energy distribution of both is similar. However, analyzing the region around (17100 m,-29100 m) in wind-tunnel and WASP plots, it can be observed that wind-tunnel plots show higher wind energy than the WASP plots. The wind tunnel results were in agreement with on-site observations, especially around the

coordinates (17100 m,-29100 m). Also, it is important to note that at the location (17250, -29200) there exists an old (more than 100 years) windmill. Further, wind-tunnel results show much higher energies, above all, at higher heights (40 m and 50 m). The plots of the numerical data show only minor changes in the wind energy values for the different heights. In fact, it can be observed that the energy decreases in some locations with increasing height.

The final Figures-26 through 33 represent the turbulence intensity distributions (TI), for the same four discrete heights and the two prevailing wind directions as the previous plots. As expected, the turbulence intensity is high in separation zones and lower regions and low in the high-elevation regions of the site. Thus, the plots are almost the "photo-negative" images of the wind energy plots, i.e., low turbulence values where the energy is high; and high turbulence values were wind energy is low. This means that for wind-turbine siting, high turbulence areas should always be avoided. The same plots also show that turbulence intensity decreases with height.

Taking into consideration that turbulence measurements do not require long-term measurement periods, as it is the case with the mean wind speed; and the results of the present investigation; it is concluded that on-site turbulence measurements combined with wind-tunnel testing, can be very valuable methods for siting wind-turbines on a large complex terrain.

Summary

Successful wind-farm development requires accurate and reliable wind-turbine siting. The siting evaluation, when performed on a very large complex terrain (several square kilometers), is an expensive and long-term process. In the present investigation, additionally to the on-site meteorological measurements, other methods were introduced for fast and reliable site evaluation: Wind-tunnel testing versus a generally accepted wind-energy calculation PC-computer program.

The UC Davis Atmospheric Boundary Layer facility, along with hot-wire anemometry, were used to take mean velocity and turbulence intensity data over a complex-terrain site-model.

On-site field turbulence measurements, using hot-film anemometry, verified the pattern of the wind-tunnel turbulence results. Also, the generally accepted WASP wind-energy-applications PC-program was used to calculate the wind-energy content over the site. The computer results were not quantitatively comparable with the wind-tunnel results, but it is believed that, in this case, the wind-tunnel data are superior to the computer results, since the simplified computer code can not simulate successfully all the details of the flow-field over the very complex terrain. Furthermore, the wind-tunnel satisfies the general similitude

parameters, which are required for correct physical modeling.

Evaluating the wind-tunnel wind-energy results in parallel with the corresponding turbulence intensity measurements, it is concluded that by excluding the high turbulence areas, the high-energy regions of the site can be outlined. Thus, turbulence measurements over a site could give a quick indication for the suitable positions of the wind-turbines in a wind-farm, taking into consideration that turbulence does not require long-term measurement periods, as it is the case with wind speed. Also, wind-tunnel simulation is a valuable tool in the process of wind energy resource assessment and wind-turbine siting.

References

1. Freris, L.L, *Wind Energy Conversion System (WECS)*, Prentice Hall Int. (UK), 1990.
2. Hiester, T.R. and Pennel, W.T., *The siting Handbook for Large WECS*, Battelle Memorial Institute, 1980.
3. Wegley, H.L., Ramsdell, J.V., Orgill, M.M., Drake, R.L., *A Siting Handbook for Small WECS*, Battelle Memorial Institute, 1980.
4. Troen, I. and Petersen, E.L., *Siting of Wind Turbines*, European Community Wind Energy Conference, Denmark, 1988.
5. Troen, I., Motensen, N.G. and Petersen, E.L., *WASP-Wind Atlas Analysis and Application Programme User's Guide*, Department of Meteorology and Wind Energy National Lab RISO, Denmark, 1990.
6. Plate, E.J., *Aerodynamic Characteristics of Atmospheric Boundary Layers,* Atomic Energy Commission, 1971.
7. Hinze, J.O., Turbulence, McGraw-Hill, 1987.
8. Migliore, P.G., Obermeier, J., White, B.R., *Wind Tunnel Testing as an Aid in Site Assessment*, Winpower '85, San Francisco, 1985.
9. Cermak, J.E., *Laboratory Simulation of the Atmospheric Boundary Layer*, AIAA Journal, No. 9, pp. 1746-1754, 1971.
10. Cermak, J.E., *Applications of Fluid Mechanics to Wind Engineering*, J. of Fluids Engineering 97, pp. 9-38, 1975a.
11. Cermac, J.E., *Simulation of Atmospheric Boundary Layers in Wind Tunnels*, Atmospheric Technology, 7, pp. 66-71, 1975b.
12. Snyder, W.H., Similarity Criteria for the Application of Fluid Models to the Study of Air Pollution Meteorology, Boundary-Layer Meteorology 3, pp. 113-134, 1972.
13. White, B.R., *Physical modeling of atmospheric flow and environmental applications*, Proceeding of the 51st Anniversary Conference of KSME, 1996.
14. Bradshaw, P., *An Introduction to Turbulence and its Measurement*, Pergamon Press, Oxford, 1971.
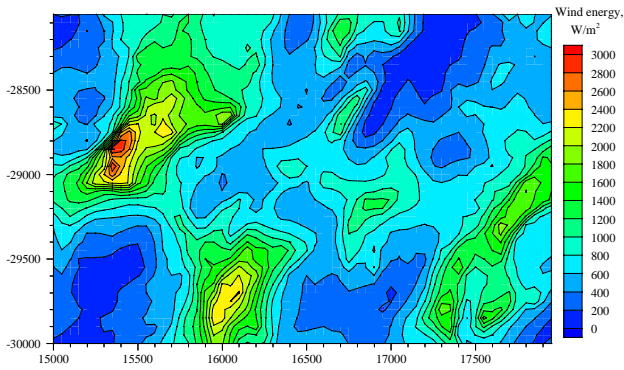
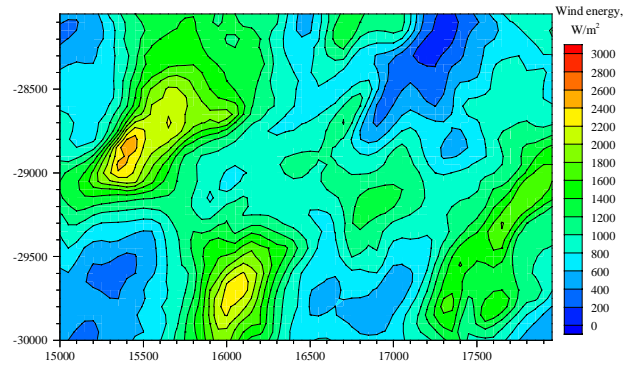*Figure-13. Wind energy distribution based on the WASP program results for 20 m above ground level.*

Figure-16. Wind energy distribution based on the WASP program results for 50 m above ground level.
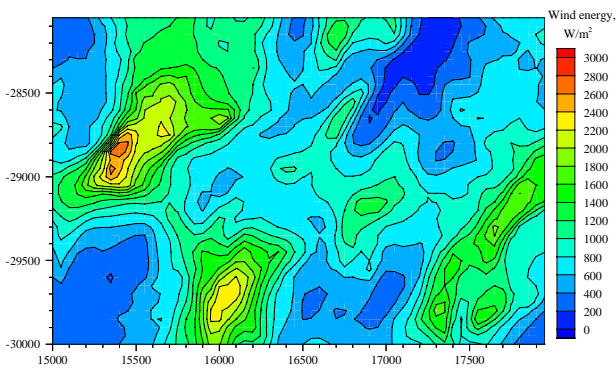

Figure-14. Wind energy distribution based on the WASP program results for 30 m above ground level.
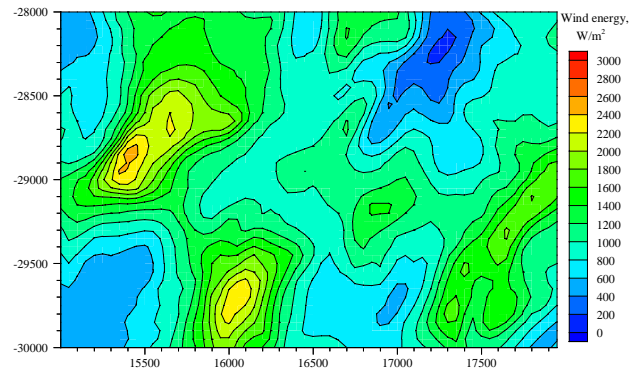

Figure-17. Wind energy distribution based on the WASP program results for 60 m above ground level.
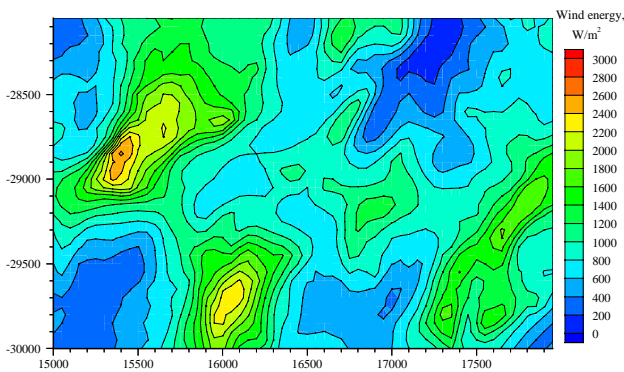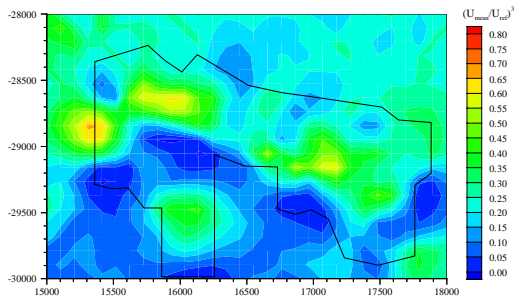

Figure-15. Wind energy distribution based on the WASP program results for 40 m above ground level.

14

American Institute of Aeronautics and Astronautics

Figure-18. Wind energy distribution for north wind at 20 m height (full-scale) in the wind tunnel
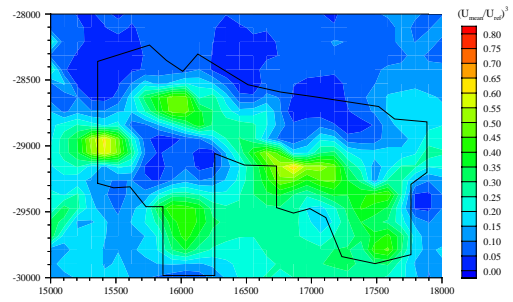
Figure-22. Wind energy distribution for south wind at 20 m height (full-scale) in the wind tunnel.
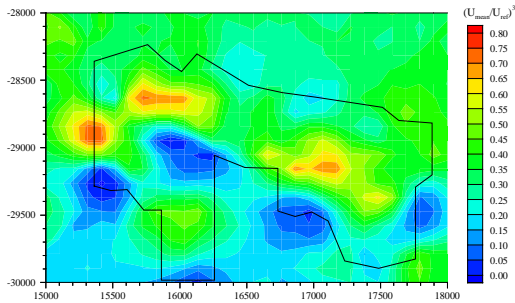
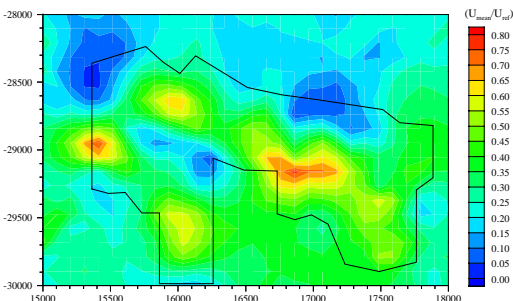*Figure-19. Wind energy distribution for north wind at 30 m height (full-scale) in the wind tunnel.*
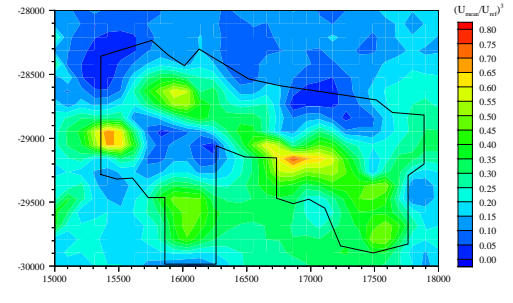
Figure-23. Wind energy distribution for south wind at 30 m height (full-scale) in the wind tunnel.
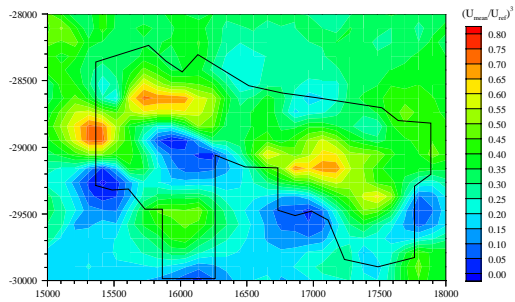
Figure-20. Wind energy distribution for north wind at 40 m height (full-scale) in the wind tunnel.
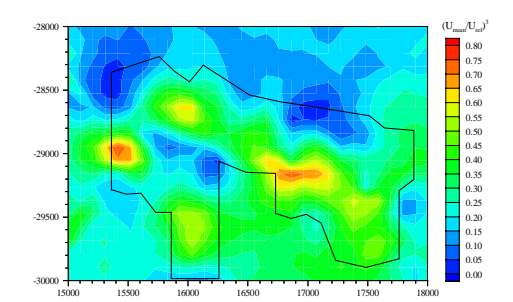
Figure-24. Wind energy distribution for south wind at 40 m height (full-scale) in the wind tunnel.
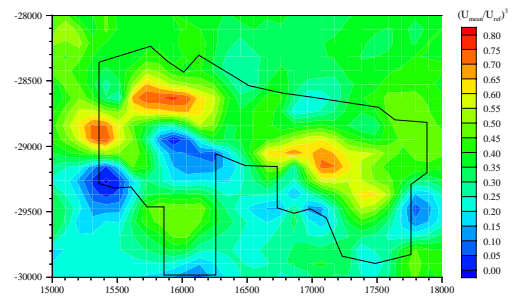
Figure-21. Wind energy distribution for north wind at 50 m height (full-scale) in the wind tunnel.

Figure-25. Wind energy distribution for south wind at 50 m height (full-scale) in the wind tunnel.

American Institute of Aeronautics and Astronautics
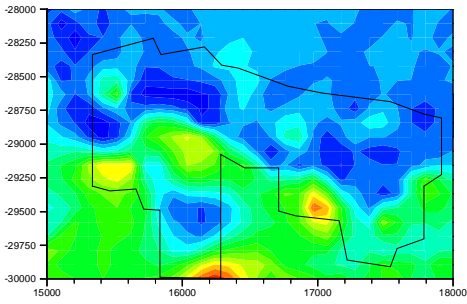
Figure-26. Turbulence intensity distribution in the wind tunnel for north wind in 20 m above ground (full-scale). TI values are in percentage (%).
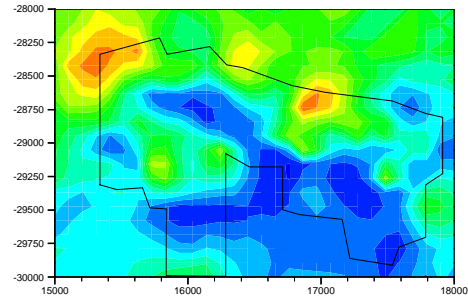

Figure-30. Turbulence intensity distribution in the wind tunnel for south wind in 20 m above ground (full-scale). TI values are in percentage (%).
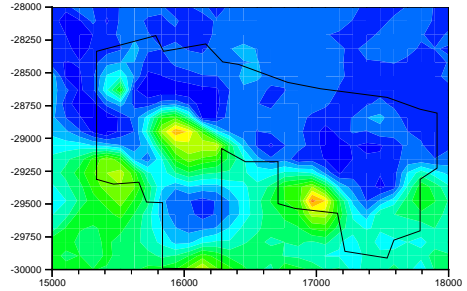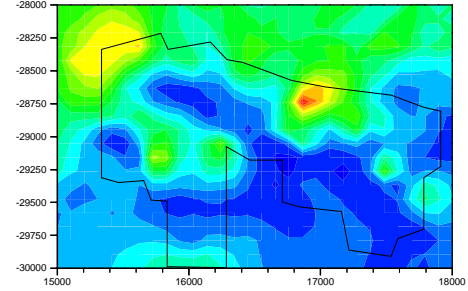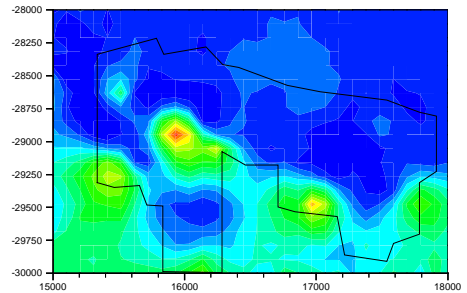

Figure-27. Turbulence intensity distribution in the wind tunnel for north wind in 30 m above ground (full-scale). TI values are in percentage (%).
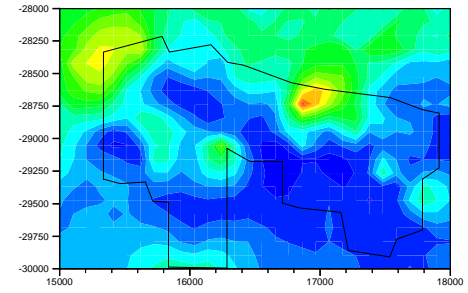

Figure-31. Turbulence intensity distribution in the wind tunnel for south wind in 30 m above ground (full-scale). TI values are in percentage (%).

Figure-28. Turbulence intensity distribution in the wind tunnel for north wind in 40 m above ground (full-scale). TI values are in percentage (%).

Figure-32. Turbulence intensity distribution in the wind tunnel for south wind in 40 m above ground (full-scale). TI values are in percentage (%).
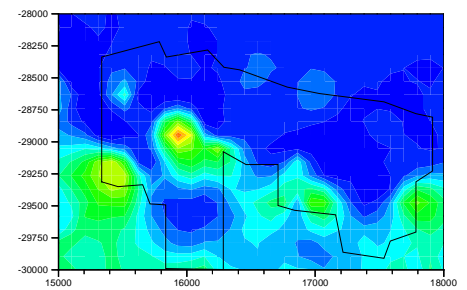

Figure-29. Turbulence intensity distribution in the wind tunnel for north wind in 50 m above ground (full-scale). TI values are in percentage (%).
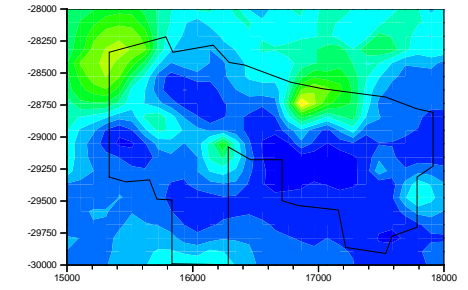

Figure-33. Turbulence intensity distribution in the wind tunnel for south wind in 50 m above ground (full-scale). TI values are in percentage (%).